ADVANCED FUNCTIONAL MATERIALS
www.afm-journal.de

Influence of Bulky Organo-Ammonium Halide Additive Choice on the Flexibility and Efficiency of Perovskite Light-Emitting Devices

*Lianfeng Zhao, Nicholas Rolston, Kyung Min Lee, Xunhua Zhao, Marcos A. Reyes-Martinez, Nhu L. Tran, Yao-Wen Yeh, Nan Yao, Gregory D. Scholes, Yueh-Lin Loo, Annabella Selloni, Reinhold H. Dauskardt, and Barry P. Rand**

Perovskite light-emitting diodes (LEDs) require small grain sizes to spatially confine charge carriers for efficient radiative recombination. As grain size decreases, passivation of surface defects becomes increasingly important. Additionally, polycrystalline perovskite films are highly brittle and mechanically fragile, limiting their practical applications in flexible electronics. In this work, the introduction of properly chosen bulky organo-ammonium halide additives is shown to be able to improve both optoelectronic and mechanical properties of perovskites, yielding highly efficient, robust, and flexible perovskite LEDs with external quantum efficiency of up to 13% and no degradation after bending for 10 000 cycles at a radius of 2 mm. Furthermore, insight of the improvements regarding molecular structure, size, and polarity at the atomic level is obtained with first-principles calculations, and design principles are provided to overcome trade-offs between optoelectronic and mechanical properties, thus increasing the scope for future highly efficient, robust, and flexible perovskite electronic device development.

1. Introduction

Organic–inorganic hybrid perovskites are an important emerging class of low cost, solution-processed semiconducting materials with promising optoelectronic properties that have achieved considerable success in lab-scale solar cells.[1–10] Beyond photovoltaics, their wavelength-tunable and narrowband emission properties enable high color purity, making perovskites attractive for light-emitting applications, such as light-emitting diodes (LEDs) and lasers.[11–18] Unlike perovskite solar cells—which favor large-grained perovskite films[19]—for light-emitting applications, perovskite grain size must be small to spatially confine charge carriers for efficient radiative recombination. Several methods have been proposed to decrease grain size, such as nanocrystal pinning[16] and nanoporous templates,[20] and external quantum efficiency (EQE) has increased from less than 1 to 11.7% in less than three years.[21,22] However, despite successful control of the grain size,[23] surface defect passivation still requires further investigation. Perovskites have unique defect tolerance properties and are insensitive to point defects inside the perovskite crystals.[24] However, there is a high density of defects at surfaces and grain boundaries of polycrystalline grains that are not electrically benign.[25–27] As grain size decreases, surface defects become increasingly important and limit device performance. To further improve device performance, passivation of defects at surfaces and grain boundaries is critical.

Mechanical robustness is another important aspect that needs to be considered for perovskite thin films, especially for applications

L. Zhao, K. M. Lee, Prof. B. P. Rand
Department of Electrical Engineering
Princeton University
Princeton, NJ 08544, USA
E-mail: brand@princeton.edu
N. Rolston, Prof. R. H. Dauskardt
Department of Materials Science and Engineering
Stanford University
Stanford, CA 94305, USA
Dr. X. Zhao, N. L. Tran, Prof. G. D. Scholes, Prof. A. Selloni
Department of Chemistry
Princeton University
Princeton, NJ 08544, USA
Dr. M. A. Reyes-Martinez, Prof. Y.-L. Loo
Department of Chemical and Biological Engineering
Princeton University
Princeton, NJ 08544, USA
Dr. Y.-W. Yeh, Prof. N. Yao
Princeton Institute for Science and Technology of Materials
Princeton University
Princeton, NJ 08544, USA
Prof. Y.-L. Loo, Prof. B. P. Rand
Andlinger Center for Energy and the Environment
Princeton University
Princeton, NJ 08544, USA
The ORCID identification number(s) for the author(s) of this article can be found under https://doi.org/10.1002/adfm.201802060.

DOI: 10.1002/adfm.201802060

 © 2018 WILEY-VCH Verlag GmbH & Co. KGaA, Weinheim

in flexible electronics. Due to the inherent highly brittle, salt-like perovskite crystal structure, perovskite films suffer from extreme mechanical fragility with low resistance to fracture.[28] Furthermore, a trade-off has been observed where improving electrical performance occurs at the expense of mechanical stability. For example, researchers have developed multiple-cation perovskites solar cells containing cesium (Cs) and formamidinium (FA), which have proven to be effective strategies to enhance power conversion efficiency to over 20%.[29,30] However, multiple-cation perovskites are more susceptible to fracture than pure methylammonium (MA) based perovskites.[31] Keeping mechanical properties in mind and developing methods that can enhance both optoelectronic properties and mechanical toughness are important to realize highly efficient, robust, and flexible perovskite devices.

Developing high-performance flexible LEDs is an important research topic with growing practical applications, such as in wearable electronics, lighting, and curved or foldable displays. However, the performance of flexible perovskite LEDs currently lags behind those on rigid substrates, with, to the best of our knowledge, a record EQE of 3.8% reported to date.[32] More effective approaches are therefore needed to simultaneously enable highly efficient, mechanically robust, and flexible perovskite LEDs. Our previous work has shown that the addition of 20 mol% bulky organo-ammonium halides can confine the crystal growth of perovskites, leading to ultrasmooth perovskite films with small crystal sizes.[11] The bulky additives serve as a matrix that covers and passivates the perovskite nanodomain surface.[33] Inspired by the idea that these additives may be helpful to both passivate surface traps and improve flexibility, in this work, we investigate the effects of five different additives—butylammonium iodide (BAI), dodecylammonium iodide (DDAI), benzylammonium iodide (PMAI), phenethylammonium iodide (PEAI), and 4-fluorobenzylammonium iodide (FPMAI)—with different molecular size, alkyl chain length, and dipole moments, on the optoelectronic and mechanical properties of perovskite films, along with their potential for flexible device applications. We find that for families of additives with alkyl chains, a trade-off exists between mechanical properties and optical properties when tuning alkyl chain length. To overcome the trade-off, increasing the polarity of the additives by introducing electron-withdrawing groups (in our case, fluorination) is a promising approach, yielding flexible perovskite LEDs with a record high EQE of 13% and no efficiency degradation after 10 000 bending cycles at a radius of 2 mm. Insight of the improvements at the atomic level is obtained with first-principles calculations, enabling the ability to provide design principles for future highly efficient, robust, and flexible perovskite electronic device development.

2. Enhancing Mechanical Stability and Optoelectronic Properties

Using a one-step perovskite film preparation procedure with 20 mol% of BAI, DDAI, PMAI, PEAI, or FPMAI additives, ultrasmooth perovskite films are achieved with similar average grain sizes in the range of 10.5–12.4 nm, as measured by transmission electron microscopy (TEM) (**Figure 1**). The additives coat the surfaces of the perovskite nanocrystals and form a matrix that hosts perovskite nanocrystals. Perovskite films without additives adopt an entirely different morphology; we observe a more conventional thin-film morphology of distinct grains defined by grain

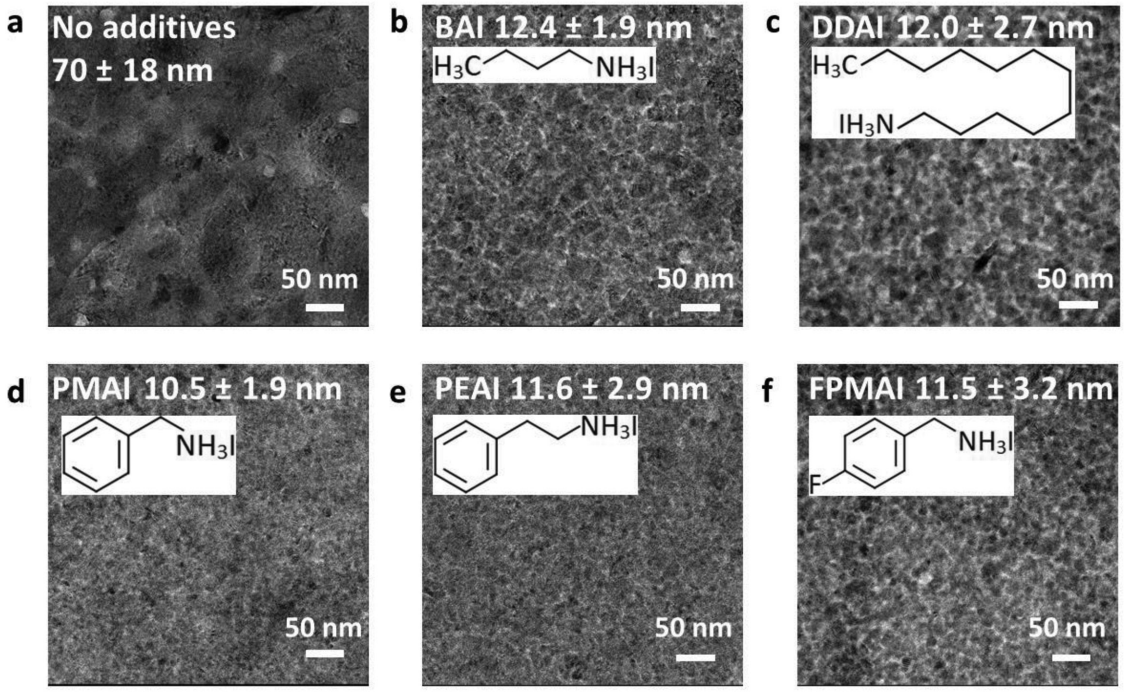

Figure 1. TEM morphology characterization for perovskite films: a) without additives, b) with BAI additives, c) with DDAI additives, d) with PMAI additives, e) with PEAI additives, and f) with FPMAI additives. The insets show the grain size distribution of each film and the corresponding chemical structures of the various additives.

© 2018 WILEY-VCH Verlag GmbH & Co. KGaA, Weinheim

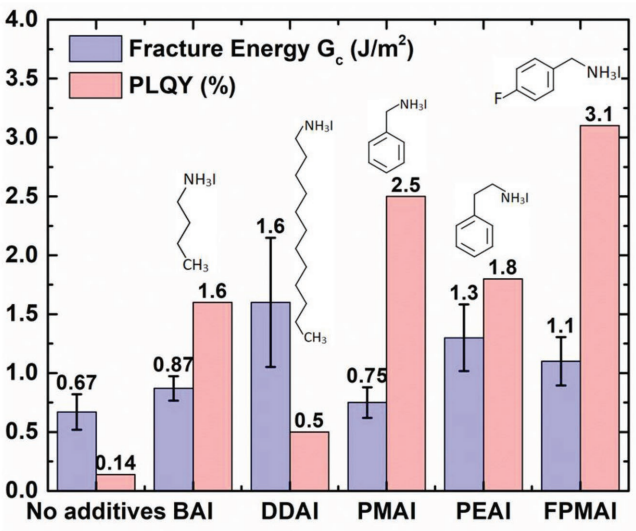

Figure 2. Fracture energy and PLQY of perovskite films without or with various additives.

boundaries, as measured by scanning electron microscopy (SEM) (Figure S1, Supporting Information). These grains possess a larger and broader size distribution of 70 ± 18 nm. Despite different grain sizes for samples with and without additives, all perovskite films maintain the same tetragonal perovskite crystal structure (Figure S2, Supporting Information), confirming that the bulky additives do not incorporate into the unit cell. It should be noted that perovskite crystal growth can only be confined through the usage of bulky additives—adding 20 mol% more methylammonium iodide (MAI) into the precursor solution still leads to large grains and rough films because MAI is small enough to fit in the perovskite crystals and thus unable to suppress the perovskite crystal growth (Figure S3, Supporting Information).

To study the effects of the bulky additives on the mechanical and optical properties of the perovskite films, we report the cohesion energy (G_c), a measurement of material resistance to crack propagation,[31] and the photoluminescence quantum yield (PLQY). As shown in **Figure 2**, all perovskite films with additives show increased G_c and PLQY compared to the control samples, suggesting that additives attach to and passivate the perovskite nanocrystal surface, enhancing both mechanical and optoelectronic properties. In fact, the cohesion energies of most perovskite devices are below 0.5 J m^{-2}, making these samples over two times more mechanically robust than other perovskite devices tested.[28,31,34] The higher fracture energy indicates that perovskite films with additives are less likely to crack compared to control films on flexible substrates subjected to mechanical stress. Notably, only bulky additives can improve the mechanical properties, while 20 mol% additional MAI will in fact lower the fracture energy (Figure S3, Supporting Information). A detailed analysis reveals two trends about the influence of these bulky additives on G_c and PLQY. First, additives with a longer alkyl chain increase G_c compared to additives with a shorter alkyl chain (1.6 J m^{-2} for DDAI compared to 0.87 J m^{-2} for BAI, 1.3 J m^{-2} for PEAI compared to 0.75 J m^{-2} for PMAI). However, the PLQY decreases for samples with longer alkyl chains (0.5% for DDAI compared to 1.6% for BAI, 1.8% for PEAI compared to 2.5% for PMAI), meaning that, for families of additives with alkyl chains, a trade-off exists between mechanical properties and optical properties when tuning alkyl chain length. Second, fluorination improves both G_c and PLQY compared to additives without fluorination (G_c of 1.1 J m^{-2} and PLQY of 3.1% for FPMAI, compared to G_c of 0.75 J m^{-2} and PLQY of 2.5% for PMAI). In this case, fluorination overcomes the trade-off between mechanical and optical properties. Notably, the impact of additive choice is more significant than the impact of film morphology on the values of G_c and PLQY. While all films with additives have similar morphology, the maximum difference of G_c and PLQY is significant (1.6 and 0.75 J m^{-2} for G_c, and 3.1 and 0.5% for PLQY). In contrast, the film morphology without additives is very distinct compared to the films with additives, while the minimum difference of G_c and PLQY is relatively small (0.67 and 0.75 J m^{-2} for G_c, 0.14 and 0.5% for PLQY). Consequently, a detailed study is warranted to understand the role of additive choice on the improved mechanical and optical properties. It should also be noted that PLQY is strongly dependent on carrier density owing to bimolecular radiative recombination in these films with low intrinsic carrier concentration.[13] A relatively low excitation power density (thus low carrier density) is used here, which is the reason for the relatively low PLQY compared to previous studies.[13]

The mechanisms for the improved mechanical and optical properties induced by these additives are different, in terms of the effects of fluorination and alkyl chain length. These are discussed in detail below.

2.1. The Effects of Fluorination and Alkyl Chain Length on Mechanical Properties

Fluorine has the highest electronegativity among all elements in the periodic table, and replacing H with F undoubtedly alters the charge distribution in the bulky molecule. As shown in **Figure 3**a, quantum chemical calculations demonstrate that the fluorinated end of FPMAI is made more negatively charged while the NH_3 end becomes more positively charged with respect to unsubstituted PMAI, resulting in an increase in the molecular dipole moment. To quantify the changes, we partition the electron density distribution with the Bader partial charge scheme and find the H of PMAI has a net charge of 0.02 e, whereas F in FPMAI has a net charge of –0.81 e.[35] The redistributed electron density in the FPMAI molecule enhances the binding energy between FPMAI molecules and the perovskite surface, and results in enhanced mechanical stability. As noted in Figure 3b, the calculated binding energy between the first monolayer of FPMAI (PMAI) and the perovskite surface is –4.33 eV (–4.28 eV), and that between the first and second monolayers of FPMAI (PMAI) is –3.52 eV (–3.40 eV). The more negative values after fluorination correlate with stronger adhesion. Further evidence for the enhanced interactions between FPMAI molecules is the presence of F—H hydrogen bonds with a length of 2.1 Å (Figure 3b). The counterpart H—H distance between PMAI molecules of 3.8 Å is much larger. Given the similar molecular structure and size between FPMAI and PMAI, van der Waals interactions between these molecules are similar, and therefore the increased binding energy

© 2018 WILEY-VCH Verlag GmbH & Co. KGaA, Weinheim

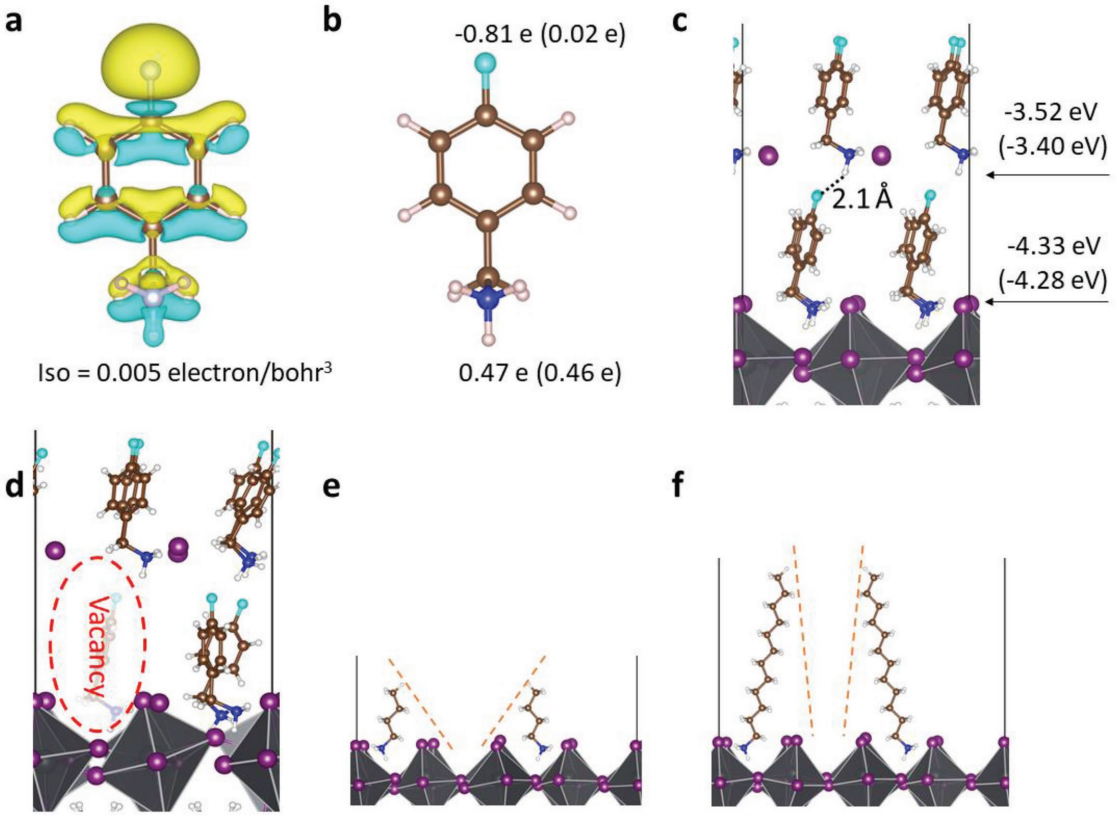

Figure 3. Calculations of the effects of fluorination and alkyl chain length on mechanical and optoelectronic properties. a) Electron density distribution difference between FPMA and PMA cations. Positive values (electron density accumulation) are plotted in yellow, negative values (electron density depletion) are plotted in green. b) Calculated Bader charge with (without) F substitution. c) Model of the interface between perovskite and the FPMA (PMA) organic additives. The numbers labeled at the interfaces are the binding energies between FPMAI (PMAI) additives and FPMAI (PMAI) with perovskite. More negative values correspond to stronger adhesion. d) Model of the interface between perovskite and the FPMA (PMA) organic additives with one additive vacancy. e) A schematic diagram of the BA/perovskite interface showing the available space for a BA molecule to attach to the perovskite surface. f) A schematic diagram of the DDA/perovskite interface, showing less available space for a DDA molecule to attach to the perovskite surface compared to BA. Carbon (C), hydrogen (H), iodine (I), nitrogen (N), fluorine (F), and lead (Pb) are represented by brown, white, purple, blue, cyan, and dark gray, respectively.

after fluorination likely accounts for the stronger mechanical properties. Our assumption of molecular–molecular interactions in this model is predicated on images (cf. Figure 1) that show that the additive capping layer on the surface of perovskite crystals is in the range of 2.5–6 nm, considerably larger than the size of the additive molecules (0.75 nm for FPMAI).

The mechanisms for the enhanced mechanical properties by longer alkyl chains, however, are distinct from the effects of fluorination. Unlike the increased binding energy between additives induced by fluorination, it has been reported that binding energy is insensitive to the alkyl chain length.[36] Instead, molecular dynamics simulations have shown that, while stretched, molecules with longer alkyl chains maintain stronger intermolecular interactions at larger stretching distance before being fully separated, whereas molecules with shorter alkyl chains will be fully separated after a shorter stretching distance.[36] Increased interaction with longer alkyl chain lengths induces larger energy dissipation processes during cohesive fracture, leading to higher G_c values, and the plastic energy dissipation results from lower stiffness of the alkyl chains compared to the perovskite.

2.2. The Effects of Fluorination and Alkyl Chain Length on Optoelectronic Properties

Time-resolved photoluminescence (TRPL) decay measurements are conducted to study the origin of the improved PLQY (Figure S4, Supporting Information). A bi-exponential decay with fast and slow components is observed for all of the films. The inclusion of additives increases both the fast and slow decay lifetimes, and the trend among different additives is the same as that for PLQY. The increased decay lifetime and PLQY indicate that the additives suppress trap-assisted nonradiative recombination. It has been reported that excess MAI in perovskite precursors forms a healing layer at grain boundaries that can suppress nonradiative recombination.[27] It is likely that the bulky additives employed here play a similar role given the common ammonium halide end group, and better surface coverage of these additives on perovskite surfaces is favorable to improve optical properties as the occupied surface sites by the additives could eliminate various surface defects, such as interstitials and antisite occupations of Pb and I.[37] Consequently, the effects of alkyl chain length and

© 2018 WILEY-VCH Verlag GmbH & Co. KGaA, Weinheim

fluorination on optoelectronic properties can be explained by the difficulty of these additives to achieve full surface coverage on the perovskite.

The effects of fluorination on surface coverage cannot be explained by molecular size due to the similar sizes of FPMAI and PMAI. Instead, the formation energy of an FPMAI or PMAI additive molecule vacancy is calculated to examine the degree to which the additives fully cover perovskite surface sites. The formation energy of an FPMAI molecule vacancy (Figure 3c) is calculated to be 3.20 eV, which is lowered to 2.04 eV for a PMAI molecule vacancy. Such a difference is in agreement with our previous results that FPMAI attaches more strongly to the crystal surface and also to other FPMAI molecules. The larger energy required for FPMAI vacancy formation indicates that it is less favorable to form a FPMAI vacancy than a PMAI vacancy, resulting in a better surface coverage of FPMAI additives than that of PMAI.

On the other hand, in terms of explaining the alkyl chain length dependence, the difficulty of these additives to achieve full surface coverage can be interpreted as a function of molecular size. As alkyl chain length increases, additives are less effective at achieving a full surface coverage. As a proof-of-concept, Figure 3e,f shows schematic diagrams comparing the available space for a BAI molecule with a shorter alkyl chain and DDAI molecule with a longer alkyl chain to attach to the perovskite surface. For DDAI, the allowed entrance cone is very narrow, making it difficult for an additional DDAI molecule to be incorporated. Additionally, the space is insufficient for the molecule to rotate freely. Once the entering molecule is oriented with the ammonium group facing away from the perovskite surface, the ammonium group no longer can readily attach to the perovskite surface by molecular rotation. We note this is a possible scenario because the hydrogen on the CH_3-end is also slightly positively charged.[38] In contrast, for smaller molecules the entrance cone is larger, and the space is sufficient for molecular rotation. As a result, the ammonium group is more likely to attach to the perovskite surface. Therefore, additives with a shorter alkyl chain are more likely to achieve a better surface coverage, minimizing surface vacancies, passivating traps, and allowing for improved optical properties.

Based on the properties detailed above, we have shown that although increasing the alkyl chain length of additives can enhance mechanical stability, it also has the unwanted effect of degrading optoelectronic functionality. To overcome the tradeoff between enhancing mechanical and optoelectronic properties, increasing the polarity of the additives by introducing electron-withdrawing groups (in our case, fluorination) is a promising approach, which can be used as an important design principle for future highly efficient, robust, and flexible perovskite electronic device development.

3. Flexible Perovskite LEDs

Flexible perovskite LEDs were fabricated with a device structure of flexible silver nanowire (AgNW) electrodes, PEDOT:PSS (60 nm), poly-TPD (25 nm), perovskite (65 nm), TPBi (40 nm), LiF (1.2 nm), and Al electrodes (Figure S5, Supporting Information), where PEDOT:PSS is poly(3,4-ethylenedioxythiophene):polystyrene sulfonate, poly-TPD is [poly[*N*,*N*′-bis(4-butylphenyl)-*N*,*N*′-bisphenylbenzidine], and TPBi is 2,2′,2″-(1,3,5-benzinetriyl)-tris(1-phenyl-1H-benzimidazole). The AgNWs are coated with titania sol-gel prior to thermal crosslinking in colorless polyimide, leading to a robust, ultrasmooth surface with a root-mean-square roughness of only 0.7 nm (Figure S6, Supporting Information). This provides a suitable platform for ultrasmooth, pinhole-free perovskite thin film deposition. Furthermore, flexible AgNW substrates prepared by this method have shown excellent mechanical flexibility, with no obvious conductivity degradation after bending for 20 000 cycles at a radius of 1 mm,[39] and have demonstrated promise as flexible electrodes for device applications.[40] An optimized balance between transmission >85% (averaged over the wavelength range from 500 to 800 nm) and sheet resistance of 25 $\Omega\,\square^{-1}$ is used here for device fabrication by tuning the concentration of AgNW inks and spin-coating cycles (**Figure 4**a). Figure 4b shows an operating flexible perovskite LED exhibiting bright red/near-infrared light emission. Figure 4c shows the measured EQE of the LEDs, with the highest EQE of 13% achieved for devices with FPMAI additives. Consistent with the PLQY results, devices utilizing additives with shorter alkyl chains show higher EQE than those with longer alkyl chains, and the highest EQE values are achieved using the fluorinated FPMAI additives. Notably, the enhanced EQE and PLQY for these films with various additives are not due to quantum confinement effects, which only manifest for nanocrystal diameters approaching the Bohr radius, ≈2.1 nm.[41] Instead, the enhancement is dominated by the passivation effects of these additives that increase the relative fraction of bimolecular radiative recombination. The current density–voltage (*J*–*V*) curves, radiance–voltage curves, EL spectra, and angle-dependent EL intensity profiles are shown in Figure S7 (Supporting Information). The EQE for flexible perovskite LEDs based on AgNW electrodes is higher than that fabricated on rigid glass/indium tin oxide (ITO) (Figure S8, Supporting Information) due to the lower work function of AgNWs compared to ITO and the enhanced light outcoupling by AgNW scattering.[40] It should be noted that we exclude the possibility that the different device performance is a result of molecular weight variations among the additives. Considering the larger molecular weight of DDAI, we reduced the DDAI additive concentration from 20 to 15, 10, and 5 mol%. If the lower EQE for the samples with DDAI additives were due to an additive overload, we would expect a higher EQE after reducing the amount of DDAI. On the contrary, lowering the DDAI concentration reduces the EQE due to inferior surface trap passivation (Figure S9, Supporting Information), proving that the low EQE for the samples with DDAI compared with the samples using other additives is not due to an overloading dose of DDAI in terms of material weight.

These flexible perovskite LEDs show excellent mechanical robustness and flexibility. Figure 4d shows a working high-efficiency FPMAI-added perovskite LED with many creases that resulted from folding five times per device area, evidence for their robustness. A bending test shows no EQE degradation after bending for 10 000 cycles at a radius of 2 mm, and the EQE maintained ≈80% after bending for 10 000 cycles at

© 2018 WILEY-VCH Verlag GmbH & Co. KGaA, Weinheim

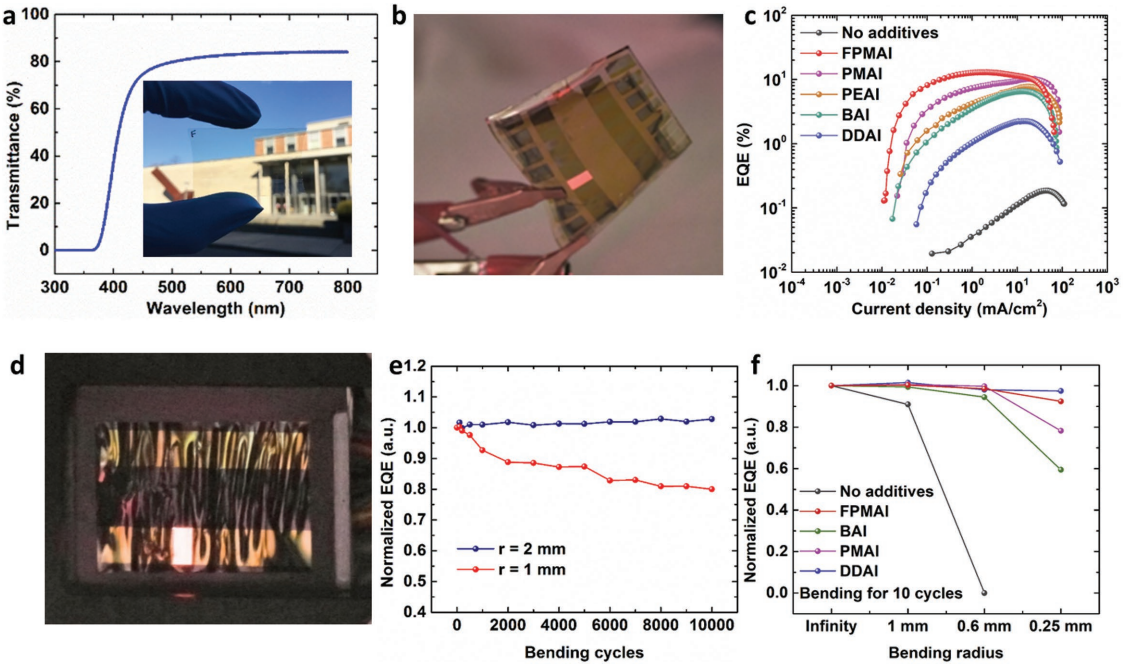

Figure 4. Flexible perovskite LED characterization and bending tests. a) Optical transmission spectrum of a flexible AgNW substrate. A photo of a flexible AgNW substrate is shown as an inset. b) A photo of a working flexible perovskite LED with FPMAI additives. c) EQE versus current density curves of perovskite LEDs without or with various additives. d) A photo of a working flexible LED with FPMAI additives after folding five times per device area. e) Normalized EQE versus bending cycles at bending radii of 1 and 2 mm for the flexible perovskite LEDs with FPMAI additives. f) Normalized EQE versus bending radius after ten bending cycles for flexible perovskite LEDs without or with various additives.

a radius of 1 mm (Figure 4e). Furthermore, no significant EQE degradation is observed when bending at extremely small radii of 1, 0.6, and 0.25 mm for ten cycles for devices with various additives (Figure 4f). In contrast, devices without additives degrade much faster than devices with additives. A detailed comparison shows that devices with longer alkyl chain additives or fluorinated additives are more robust than those with shorter alkyl chain additives or nonfluorinated additives, which are consistent with the fracture energy results of these perovskite films. In addition to the bending tests, the fracture-onset strains of perovskite films are measured using a combined wrinkling–cracking method based on film-elastomer bilayer stretching.[42] It is found that the fracture-onset strain of the films with FPMAI additives is ≈2.7% (Figure S10, Supporting Information), similar to flexible organic materials such as poly(3-hexylthiophene) films with a 15 kDa molecular weight.[43] In contrast, perovskite films without additives have a fracture-onset strain of about 1.4%, similar to more brittle inorganic materials such as SiN_x, SiO_x, and Ta.[42,44] The increased fracture-onset strain for the perovskite films with additives is not surprising given the correlation between fracture-onset strain and fracture energy.[45] In addition, thanks to the strong adhesion of the perovskite materials to the adjacent layers, our device structure is robust against delamination at extremely small bending radii. These mechanical properties including flexibility combined with high resistance to fracture and delamination make our perovskite LEDs an ideal structure and platform for applications in flexible electronics.

4. Conclusion

In summary, we have described and demonstrated a facile method to improve both the optoelectronic and mechanical properties of perovskites by additive engineering, yielding highly efficient, robust, and flexible perovskite LEDs with an EQE of 13% and no degradation after 10 000 bending cycles at a radius of 2 mm. We find that for families of additives with alkyl chains, a trade-off exists between mechanical properties and optical properties when tuning alkyl chain length. To overcome the trade-off, increasing the polarity of the additives by introducing electron-withdrawing groups (in our case, fluorination) is a promising approach. Insight of the improvements at the atomic level is obtained with first-principles calculations, through which we provide design principles for future highly efficient, robust, and flexible perovskite electronic device development.

5. Experimental Section

Silver Nanowire Substrate Preparation: A rigid glass substrate was used as a carrier substrate to deposit 30 nm diameter AgNWs by spin-coating. The AgNWs used in this work were on average 30 nm in diameter and 100–200 µm in length, purchased from ACS Materials. This AgNW ink was dispersed in ethanol to yield a concentration of ≈2.5 wt%. Titania sol-gel was synthesized,[39] and a thin ≈2 nm layer was spin-coated on the AgNW network to prevent them from breaking up during thermal imidization of colorless polyimide. 10 wt% colorless polyimide precursors were synthesized,[40] and then blade-coated on the carrier

© 2018 WILEY-VCH Verlag GmbH & Co. KGaA, Weinheim

substrate which was then imidized (20 min at 160 °C followed by 20 min at 360 °C). Finally, the conductive polyimide substrate (≈15 µm) was delaminated from the glass substrate.

Material Synthesis: MAI, BAI, DDAI, PMAI, PEAI, and FPMAI were synthesized by mixing methylamine (MA), butylamine (BA), dodecylamine (DDA), benzylamine (PMA), phenethylamine (PEA), and 4-fluorobenzylamine (FPMA) (Sigma Aldrich) with HI (Sigma Aldrich) in a 1:1 molar ratio, respectively. The reaction was performed in an ice bath while stirring for 3 h. The solvent of the resulting solution was evaporated using a rotary evaporator. The MAI, BAI, DDAI, PMAI, PEAI, and FPMAI were recrystallized from an isopropyl alcohol:toluene mixture. Finally, the large crystals were filtered and dried under low heat. The recrystallization, filtration, and drying were performed inside a N_2 filled glove box.

Flexible Perovskite LED Fabrication: PEDOT:PSS with 0.01% (volume ratio) polyethylene glycol *tert*-octylphenyl ether (Triton X-100, Sigma Aldrich) was spin-coated on the prepared AgNW embedded polyimide substrates and annealed at 130 °C for 10 min. Triton X-100 acts as a surfactant to improve wetting on the polyimide substrates. Then, poly-TPD (6 mg mL^{-1} in chlorobenzene) was spin-coated on the PEDOT:PSS layer at 1500 rpm for 70 s followed by thermal annealing at 150 °C for 20 min. Poly-TPD was then treated with O_2 plasma for 4 s to improve wetting. The perovskite precursor solution was prepared by mixing PbI_2 and MAI in DMF (Sigma Aldrich, 99.8% anhydrous) in a 1:1 molar ratio to obtain 0.4 M $MAPbI_3$ solution. For solutions with BAI, DDAI, PMAI, PEAI, or FPMAI, 20 mol% additives were mixed with the stoichiometric $MAPbI_3$ perovskite precursors. Perovskite films with or without additives were deposited on poly-TPD by spin-coating at 6000 rpm. A solvent exchange step was performed after 3.5 s by dropping toluene on the spinning samples. Then, samples were annealed at 70 °C for 5 min. TPBi, LiF, and Al layers were thermally evaporated with thicknesses of 40, 1.2, and 100 nm, respectively. Device area was 0.1 cm^2.

Material and Device Characterization: The film surface morphologies were surveyed by an FEI Verios 460 XHR SEM. The crystal structures of the films were studied by using a Bruker D8 Discover X-ray diffractometer with incident wavelength of 0.154 nm. The high-resolution TEM (HRTEM) images were carried out in an FEI Talos (S)TEM at 200 kV. Cross-section lamella samples of the flexible LEDs were prepared by an FEI Helios DualBeam microscope. The atomic force microscopy (AFM) measurements were performed with a Bruker Dimension ICON3 atomic force microscope. The TRPL measurements were carried out using an FLS980 spectrometer (Edinburgh Instruments). Samples were excited at 634.8 nm by a pulsed laser diode with a 500 ns pulse period. The PLQY was measured using a Petite integrating sphere coupled to the PTI QuantaMaster 400 Steady State Fluorometer system. An excitation wavelength of 450 nm was used. The following settings were kept the same for all films: bandpass values of 5 nm for both the excitation and emission slits, step increments of 1 nm, and integration times of 0.5 s per data point. The excitation intensity was ≈0.3 mW cm^{-2}. The transmittance spectra were measured using an Agilent Cary 5000 UV–vis–NIR spectrophotometer. Perovskite LEDs were characterized in a N_2 glove box using a custom motorized goniometer consisting of a Keithley 2400 sourcemeter unit, a picoammeter (4140B, Agilent), a calibrated Si photodiode (FDS-100-CAL, Thorlabs), and a calibrated fiber optic spectrophotometer (UVN-SR, StellarNet Inc.).

Fracture Energy Testing: The mechanical testing was performed using double cantilever beam (DCB) specimens fabricated by sandwiching the perovskite films of interest between glass beams with a thin, brittle epoxy (E-20NS, Hysol) cured overnight under pressure in a N_2 glove box at 25 °C. Before bonding, a protective, cross-linked PTAA polymer layer[34] at a concentration of 15 mg mL^{-1} (Solaris Chem.) with 3 mg mL^{-1} of 1,3,5,7-tetrakis-(*p*-benzylazide)-adamantane was spin-coated onto the perovskite films, and a metal barrier film (Ti/Al) was e-beam evaporated onto the PTAA to prevent epoxy diffusion. Specimens were cleaned with a razor blade after curing to remove epoxy from the edges of the beams. DCB specimens were tested under displacement control in a thin-film mechanical testing system (Delaminator DTS, Menlo Park, CA) from which a load, P, versus displacement, Δ, curve was recorded. The fracture energy, G_c (J m^{-2}), was calculated in terms of the critical value of the applied strain energy release rate, G. G_c can be formulated in terms of the critical load, P_c, at which crack growth initiates, the crack length, a, the plane-strain elastic modulus, E', of the substrates and the specimen dimensions: width, B and half-thickness, h. G_c was calculated from Equation (1)[46]

$$G_c = \frac{12P_c^2a^2}{B^2E'h^3}\left(1+0.64\frac{h}{a}\right)^2 \tag{1}$$

An approximation of the crack length was empirically found from a measurement of the elastic compliance, $d\Delta/dP$, using the compliance relationship in Equation (2)

$$a = \left(\frac{d\Delta}{dP}\times\frac{BE'h^3}{8}\right)^{1/3} - 0.64\times h \tag{2}$$

All G_c testing was carried out in standard laboratory conditions at ≈25 °C and ≈40% R.H. The specimen was pulled apart with a displacement rate of 1.0 µm s^{-1} until reaching P_c before slightly unloading to calculate $d\Delta/dP$. The specimens were then loaded again to P_c and the process repeated until the crack propagated through the entire length of the perovskite film.

Fracture-Onset Strain Measurement: To measure the fracture properties of thin films, combined wrinkling–cracking method based on film-elastomer bilayer stretching was employed as introduced by Stafford and co-workers.[42] Perovskite films were spin-coated on glass/poly(9-vinylcarbazole) (PVK) substrates using the same procedure indicated above. Samples were then immersed in chlorobenzene and elastomeric polydimethylsiloxane (PDMS) substrates were used to pick up the perovskite films from chlorobenzene. The PVK layer is used as a sacrificial layer, which is soluble in chlorobenzene to facilitate the transfer of perovskite films to a PDMS substrate for stretching experiments. PDMS substrates were cut into a dog-bone shape (20 × 5 mm gauge dimensions) prior to tensile experiments to ensure homogenous strain distribution across the film. Uniaxial tensile strain was applied using a custom-made manual strain stage. Three characteristic fracture regimes can be observed as the tensile strain increases. First, multiple cracks appear at random locations and with varying fragment width (d) mainly due to film heterogeneities such as nanometric variations in thickness. In the second regime, fragments fracture at their midpoints. In this regime, the distribution of d is narrower and each fragment is divided into two subfragments when the strain is doubled. In the third regime, subfragmentation stops. In this regime, the stress transferred from the substrate to the film is not enough to continue the fracture process and delamination of wrinkles is observed. In this technique, the average fragment width is defined by[42]

$$\langle d\rangle = \frac{2h_f\sigma^*}{E_s\bar{\varepsilon}} \tag{3}$$

where h_f is the film thickness, σ^* is the fracture strength, E_s is the substrate modulus, and $\bar{\varepsilon}$ is the strain after the onset of fracture ε^*. ε^* is obtained from the x-intercept of a linear fit of the rescaled crack density, $2h_f/\langle d\rangle E_s$, as a function of applied ε.

Computational Details: The perovskite surface was represented by a four-layer slab of the crystal. The interface was modeled by adding two monolayers of the additives (FPMAI or PMAI). The slab was stoichiometric and neutral in charge. The total energies and electronic structures were calculated with the first-principles code Quantum-espresso[47] and the GGA functional PBE[48] was used. A Wavefunction (charge density) cutoff value of 40 (320) Rydberg and 3 × 3 × 1 k-grid were used in all calculations after testing larger values. Dipole-correction in the surface normal direction was employed for all calculations.[49] The binding energy was defined as

© 2018 WILEY-VCH Verlag GmbH & Co. KGaA, Weinheim

$$E_{\text{bind}} = (E_{\text{aft.}} - E_{\text{bef.}} - nE_{\text{adsobates}})/n \quad (4)$$

In the first layer adsorption, for instance, $E_{\text{bef.}}$ is the total energy without FPMAI (PMAI) adsorption, $E_{\text{aft.}}$ is the total energy with one monolayer FPMAI (PMAI) adsorption, and $E_{\text{adsobates}}$ is the total energy sum of the isolated additive molecules. In this model, $n = 4$. Formation energy of a PMAI (FPMAI) molecule vacancy can be evaluated by $\Delta H_{\text{form}} = E_{\text{vacancy}} - E_{\text{pristine}} + \sum n_i E_i + \sum n_i \mu_i$, where E_{vacancy} and E_{pristine} are total energies of two monolayer adsorptions after and before the formation of a PMAI (FPMAI) molecule vacancy, E_i and μ_i are the total energy and chemical potential of the i atom or molecule. Typical chemical potentials $\mu_{\text{PMA}} = \mu_{\text{FPMA}} = -2.41$ eV, $\mu_{\text{I}} = -0.60$ eV are used in the calculations.[50]

Supporting Information

Supporting Information is available from the Wiley Online Library or from the author.

Acknowledgements

L.Z. and B.P.R. conceived the idea and designed the experiments. L.Z. developed the flexible perovskite LED fabrication process, characterized the LEDs, conducted the XRD, FIB, SEM, TEM, transmittance, and TRPL measurements. N.R. and R.H.D. conducted the fracture energy measurements. K.M.L. prepared the flexible silver nanowire substrates. X.Z. and A.S. conducted the first-principles calculations. M.A.R.-M. and Y.-L.L. measured the critical fracture strains. N.L.T. and G.D.S. measured the PLQY. Y.-W.Y. and N.Y. conducted the AFM measurements and assisted with the TEM measurements. L.Z. and B.P.R. wrote the manuscript. All authors discussed the results and contributed to the manuscript. The authors acknowledge research funding for this work from the ONR Young Investigator Program (Award No. N00014-17-1-2005). N.R. and R.H.D. were supported by a grant from the Bay Area Photovoltaics Consortium under Award No. DE-EE0004946. X.Z. and A.S. acknowledge use of the TIGRESS High-Performance Computer Center at Princeton University. N.R. acknowledges additional support from the National Science Foundation Graduate Research Fellowship under Award No. DGE-1656518. The authors acknowledge the usage of Princeton's Imaging and Analysis Center which is partially supported by Princeton Center for Complex Materials from National Science Foundation (NSF)-MRSEC program (DMR-1420541).

Conflict of Interest

The authors declare no conflict of interest.

Keywords

flexible light-emitting diodes, metal halide perovskite, perovskite light-emitting diodes

Received: March 22, 2018
Revised: April 24, 2018
Published online: June 14, 2018

[1] N.-G. Park, M. Grätzel, T. Miyasaka, K. Zhu, K. Emery, *Nat. Energy* **2016**, *1*, 16152.
[2] M. A. Green, A. Ho-Baillie, H. J. Snaith, *Nat. Photonics* **2014**, *8*, 506.
[3] H. Tsai, W. Nie, J.-C. Blancon, C. C. Stoumpos, R. Asadpour, B. Harutyunyan, A. J. Neukirch, R. Verduzco, J. J. Crochet, S. Tretiak, L. Pedesseau, J. Even, M. A. Alam, G. Gupta, J. Lou, P. M. Ajayan, M. J. Bedzyk, M. G. Kanatzidis, A. D. Mohite, *Nature* **2016**, *536*, 312.
[4] M. Liu, M. B. Johnston, H. J. Snaith, *Nature* **2013**, *501*, 395.
[5] N. J. Jeon, J. H. Noh, Y. C. Kim, W. S. Yang, S. Ryu, S. I. Seok, *Nat. Mater.* **2014**, *13*, 897.
[6] B. Saparov, D. B. Mitzi, *Chem. Rev.* **2016**, *116*, 4558.
[7] G. E. Eperon, T. Leijtens, K. A. Bush, R. Prasanna, T. Green, J. T.-W. Wang, D. P. McMeekin, G. Volonakis, R. L. Milot, R. May, A. Palmstrom, D. J. Slotcavage, R. A. Belisle, J. B. Patel, E. S. Parrott, R. J. Sutton, W. Ma, F. Moghadam, B. Conings, A. Babayigit, H.-G. Boyen, S. Bent, F. Giustino, L. M. Herz, M. B. Johnston, M. D. McGehee, H. J. Snaith, *Science* **2016**, *354*, 861.
[8] L. Qiu, L. K. Ono, Y. Qi, *Mater. Today Energy* **2017**, *7*, 169.
[9] J. Huang, Y. Yuan, Y. Shao, Y. Yan, *Nat. Rev. Mater.* **2017**, *2*, 17042.
[10] T. M. Brenner, D. A. Egger, L. Kronik, G. Hodes, D. Cahen, *Nat. Rev. Mater.* **2016**, *1*, 15007.
[11] Z. Xiao, R. A. Kerner, L. Zhao, N. L. Tran, K. M. Lee, T.-W. Koh, G. D. Scholes, B. P. Rand, *Nat. Photonics* **2017**, *11*, 108.
[12] Y. Jia, R. A. Kerner, A. J. Grede, B. P. Rand, N. C. Giebink, *Nat. Photonics* **2017**, *11*, 784.
[13] M. Yuan, L. N. Quan, R. Comin, G. Walters, R. Sabatini, O. Voznyy, S. Hoogland, Y. Zhao, E. M. Beauregard, P. Kanjanaboos, Z. Lu, D. H. Kim, E. H. Sargent, *Nat. Nanotechnol.* **2016**, *11*, 872.
[14] H. Zhu, Y. Fu, F. Meng, X. Wu, Z. Gong, Q. Ding, M. V. Gustafsson, M. T. Trinh, S. Jin, X. Y. Zhu, *Nat. Mater.* **2015**, *14*, 636.
[15] L. Zhang, X. Yang, Q. Jiang, P. Wang, Z. Yin, X. Zhang, H. Tan, Y. Yang, M. Wei, B. R. Sutherland, E. H. Sargent, J. You, *Nat. Commun.* **2017**, *8*, 15640.
[16] H. Cho, S.-H. Jeong, M.-H. Park, Y.-H. Kim, C. Wolf, C.-L. Lee, J. H. Heo, A. Sadhanala, N. Myoung, S. Yoo, *Science* **2015**, *350*, 1222.
[17] S. Yakunin, L. Protesescu, F. Krieg, M. I. Bodnarchuk, G. Nedelcu, M. Humer, G. De Luca, M. Fiebig, W. Heiss, M. V. Kovalenko, *Nat. Commun.* **2015**, *6*, 8056.
[18] S. Chen, K. Roh, J. Lee, W. K. Chong, Y. Lu, N. Mathews, T. C. Sum, A. Nurmikko, *ACS Nano* **2016**, *10*, 3959.
[19] H. D. Kim, H. Ohkita, H. Benten, S. Ito, *Adv. Mater.* **2016**, *28*, 917.
[20] S. Demchyshyn, J. M. Roemer, H. Groiß, H. Heilbrunner, C. Ulbricht, D. Apaydin, A. Böhm, U. Rütt, F. Bertram, G. Hesser, M. C. Scharber, N. S. Sariciftci, B. Nickel, S. Bauer, E. D. Głowacki, M. Kaltenbrunner, *Sci. Adv.* **2017**, *3*, e1700738.
[21] Z.-K. Tan, R. S. Moghaddam, M. L. Lai, P. Docampo, R. Higler, F. Deschler, M. Price, A. Sadhanala, L. M. Pazos, D. Credgington, *Nat. Nanotechnol.* **2014**, *9*, 687.
[22] N. Wang, L. Cheng, R. Ge, S. Zhang, Y. Miao, W. Zou, C. Yi, Y. Sun, Y. Cao, R. Yang, Y. Wei, Q. Guo, Y. Ke, M. Yu, Y. Jin, Y. Liu, Q. Ding, D. Di, L. Yang, G. Xing, H. Tian, C. Jin, F. Gao, R. H. Friend, J. Wang, W. Huang, *Nat. Photonics* **2016**, *10*, 699.
[23] H. Huang, J. Raith, S. V. Kershaw, S. Kalytchuk, O. Tomanec, L. Jing, A. S. Susha, R. Zboril, A. L. Rogach, *Nat. Commun.* **2017**, *8*, 996.
[24] W.-J. Yin, T. Shi, Y. Yan, *Appl. Phys. Lett.* **2014**, *104*, 063903.
[25] X. Zheng, B. Chen, J. Dai, Y. Fang, Y. Bai, Y. Lin, H. Wei, Xiao C. Zeng, J. Huang, *Nat. Energy* **2017**, *2*, 17102.
[26] H. Tan, A. Jain, O. Voznyy, X. Lan, F. P. García de Arquer, J. Z. Fan, R. Quintero-Bermudez, M. Yuan, B. Zhang, Y. Zhao, F. Fan, P. Li, L. N. Quan, Y. Zhao, Z.-H. Lu, Z. Yang, S. Hoogland, E. H. Sargent, *Science* **2017**, *355*, 722.
[27] D.-Y. Son, J.-W. Lee, Y. J. Choi, I.-H. Jang, S. Lee, P. J. Yoo, H. Shin, N. Ahn, M. Choi, D. Kim, N.-G. Park, *Nat. Energy* **2016**, *1*, 16081.
[28] N. Rolston, B. L. Watson, C. D. Bailie, M. D. McGehee, J. P. Bastos, R. Gehlhaar, J.-E. Kim, D. Vak, A. T. Mallajosyula, G. Gupta, A. D. Mohite, R. H. Dauskardt, *Extreme Mech. Lett.* **2016**, *9*, 353.

© 2018 WILEY-VCH Verlag GmbH & Co. KGaA, Weinheim

[29] M. Saliba, T. Matsui, J.-Y. Seo, K. Domanski, J.-P. Correa-Baena, M. K. Nazeeruddin, S. M. Zakeeruddin, W. Tress, A. Abate, A. Hagfeldt, M. Gratzel, *Energy Environ. Sci.* **2016**, *9*, 1989.
[30] D. P. McMeekin, G. Sadoughi, W. Rehman, G. E. Eperon, M. Saliba, M. T. Hörantner, A. Haghighirad, N. Sakai, L. Korte, B. Rech, M. B. Johnston, L. M. Herz, H. J. Snaith, *Science* **2016**, *351*, 151.
[31] N. Rolston, A. D. Printz, J. M. Tracy, H. C. Weerasinghe, D. Vak, L. J. Haur, A. Priyadarshi, N. Mathews, D. J. Slotcavage, M. D. McGehee, R. E. Kalan, K. Zielinski, R. L. Grimm, H. Tsai, W. Nie, A. D. Mohite, S. Gholipour, M. Saliba, M. Grätzel, R. H. Dauskardt, *Adv. Energy Mater.* **2018**, *8*, 1702116.
[32] M. Prezioso, F. Merrikh-Bayat, B. D. Hoskins, G. C. Adam, K. K. Likharev, D. B. Strukov, *Nature* **2015**, *521*, 61.
[33] L. Zhao, Y.-W. Yeh, N. L. Tran, F. Wu, Z. Xiao, R. A. Kerner, Y. L. Lin, G. D. Scholes, N. Yao, B. P. Rand, *ACS Nano* **2017**, *11*, 3957.
[34] B. Watson, N. Rolston, K. A. Bush, L. Taleghani, R. H. Dauskardt, *J. Mater. Chem. A* **2017**, *5*, 19267.
[35] W. Tang, E. Sanville, G. Henkelman, *J. Phys.: Condens. Matter* **2009**, *21*, 084204.
[36] Y. Chen, J. Y. H. Chia, Z. C. Su, T. E. Tay, V. B. C. Tan, *Polymer* **2013**, *54*, 766.
[37] J. M. Ball, A. Petrozza, *Nat. Energy* **2016**, *1*, 16149.
[38] P. Lazzeretti, R. Zanasi, W. T. Raynes, *J. Chem. Phys.* **1987**, *87*, 1681.
[39] J. A. Spechler, T.-W. Koh, J. T. Herb, B. P. Rand, C. B. Arnold, *Adv. Funct. Mater.* **2015**, *25*, 7428.
[40] K. M. Lee, R. Fardel, L. Zhao, C. B. Arnold, B. P. Rand, *Org. Electron.* **2017**, *51*, 471.
[41] Y. Hassan, Y. Song, R. D. Pensack, A. I. Abdelrahman, Y. Kobayashi, M. A. Winnik, G. D. Scholes, *Adv. Mater.* **2016**, *28*, 566.
[42] J. Y. Chung, J.-H. Lee, K. L. Beers, C. M. Stafford, *Nano Lett.* **2011**, *11*, 3361.
[43] D. Rodriquez, J.-H. Kim, S. E. Root, Z. Fei, P. Boufflet, M. Heeney, T.-S. Kim, D. J. Lipomi, *ACS Appl. Mater. Interfaces* **2017**, *9*, 8855.
[44] J. Andersons, J. Modniks, Y. Leterrier, G. Tornare, P. Dumont, J. A. E. Månson, *Theor. Appl. Fract. Mech.* **2008**, *49*, 151.
[45] N. Balar, B. T. O'Connor, *Macromolecules* **2017**, *50*, 8611.
[46] M. F. Kanninen, *Int. J. Fract.* **1973**, *9*, 83.
[47] G. Paolo, B. Stefano, B. Nicola, C. Matteo, C. Roberto, C. Carlo, C. Davide, L. C. Guido, C. Matteo, D. Ismaila, C. Andrea Dal, G. Stefano de, F. Stefano, F. Guido, G. Ralph, G. Uwe, G. Christos, K. Anton, L. Michele, M.-S. Layla, M. Nicola, M. Francesco, M. Riccardo, P. Stefano, P. Alfredo, P. Lorenzo, S. Carlo, S. Sandro, S. Gabriele, P. S. Ari, S. Alexander, U. Paolo, M. W. Renata, *J. Phys.: Condens. Matter* **2009**, *21*, 395502.
[48] J. P. Perdew, K. Burke, M. Ernzerhof, *Phys. Rev. Lett.* **1996**, *77*, 3865.
[49] L. Bengtsson, *Phys. Rev. B* **1999**, *59*, 12301.
[50] W.-J. Yin, T. Shi, Y. Yan, *J. Phys. Chem. C* **2015**, *119*, 5253.

© 2018 WILEY-VCH Verlag GmbH & Co. KGaA, Weinheim